Adaptive Robust Impedance Control for an Ear Surgical Device With Soft Interaction

Zhao Feng , Wenyu Liang , *Member, IEEE*, Jie Ling , *Member, IEEE*, Xiaohui Xiao , *Member, IEEE*, Kok Kiong Tan, and Tong Heng Lee , *Member, IEEE*

Abstract—The required suitably soft-contact interaction in certain surgical device applications brings great challenges on the force and position control because the soft-contact environment is nonlinear, viscoelastic, and inhomogeneous. In this article, a novel adaptive robust control approach, namely adaptive integral terminal sliding-mode-based impedance control (AITSMIC), is formulated to simultaneously regulate and control the position and force for a piezoactuated ear surgical device with soft interaction. First, the target impedance's steady-state performance is discussed by utilizing the nonlinear Hunt–Crossley model. To achieve the desired impedance, an integral terminal sliding manifold based on the auxiliary variable containing the impedance error is proposed to improve tracking performance and obtain the required finite-time convergence. Furthermore, an adaptive law is designed to get rid of system nonlinearities, uncertainties and disturbances, and to retain high robustness. The stability of the proposed control system is proven via the Lyapunov theory. Significantly, implementing the AITSMIC is straightforward, where only essentially one uniform controller is applied. Finally, several experiments are conducted to evaluate the effects of associated impedance parameters, verify the force-tracking performance and validate the suitably practical application of AITSMIC on the procedure of ear surgery with soft interaction. The results show that excellent tracking performance and successful operation are achieved by the proposed controller.

Index Terms—Adaptive control, compliance control, medical devices, piezoelectric devices, robustness.

Zhao Feng was with the School of Power and Mechanical Engineering, Wuhan University, Wuhan 430072, China and also with the Department of Electrical and Computer Engineering, National University of Singapore, 117576, Singapore, and is now with the Faculty of Science and Technology, University of Macau, Macao 999078, China (e-mail: zhaofeng@um.edu.mo).

Wenyu Liang is with the Department of Electrical and Computer Engineering, National University of Singapore, , Singapore 117576 and also with the Institute for Infocomm Research, A*STAR, Singapore 138632, Singapore (e-mail: liangwenyu@u.nus.edu).

Jie Ling is with the College of Mechanical & Electrical Engineering, Nanjing University of Aeronautics and Astronautics, Nanjing 210016, China (e-mail: meejling@nuaa.edu.cn).

Xiaohui Xiao is with the School of Power and Mechanical Engineering, Wuhan University, Wuhan 430072, China (e-mail: xhxiao@whu.edu.cn).

Kok Kiong Tan is with the ZAI Company, Singapore 737960 (e-mail: kktan@nus.edu.sg).

Tong Heng Lee is with the Department of Electrical and Computer Engineering, National University of Singapore, Singapore 117576, Singapore (e-mail: eleleeth@nus.edu.sg).

Color versions of one or more figures in this article are available at https://doi.org/10.1109/TMECH.2021.3087014.

Digital Object Identifier 10.1109/TMECH.2021.3087014

I. INTRODUCTION

WITH the rapid development and real-world applicability of robotic technologies, interaction with the environment becomes an essential part of the overall process to carry out particular tasks successfully, such as series elastic actuators [1], cell microinjection [2], and robot-assisted surgeries [3]. When these devices get in contact with the environment, an interaction force arises, which would affect the success of the task. Under these circumstances, it is, thus, particularly important that the interaction force should be well-controlled to guarantee the safety of both the device and contact environment, for instances of human–robot interaction [4]. In addition, the overall tasks may also need the accurate position tracking. This is certainly the situation for the ear robotic surgery [5], where there is an interaction with the human tissues. Hence, a well-designed controller plays a very major role to properly and accurately regulate the interaction force and position of the device during the task at the same time. This is particularly important in ear surgery manipulation that requires a certain accuracy of both force and position [3], [5].

To handle the interaction problem, force regulation is a possible way to assure the correct contact between the device and environment. Thus, Zarrouk *et al.* designed a model reference adaptive controller that is suitable for the force control of beating heart surgery in [6]. In [7], Lee *et al.* proposed and implemented an inversion-free force-tracking controller without complicated modeling on a variable physical damping actuator mechanism driven by piezoelectric actuators. However, the performance may be deteriorated significantly when contacting soft environment although suitable individual force controllers can achieve low force overshoot and fast response; and this would be particularly so if the contact model is not built accurately enough [8]. Besides that, with pure force controllers, the actuated device's position is typically uncontrolled and unconstrained so that the desired location cannot be reached by the actuated

device, often-times part of the overall task in some situations, like the ear surgery in [5].

In moving beyond pure force control, it is worth noting that employing the hybrid position/force control approach [9] can realize both position regulation and force regulation. The hybrid approach includes the position controller track position and force controller to track force, respectively. Thus, Wang *et al.* combined an adaptive sliding-mode position controller and a proportional–integral–derivative (PID) force controller for zebrafish embryos penetration in [10]. In [11], Liang and Tan applied a hybrid position/force controller approach with a suitably optimized algorithm on an ear surgical device. However, in the operating process for such a hybrid approach, the required switching between two different control laws may give rise to instability of the overall system [12]; and the hybrid approach also need more parameters to be tuned for implementation.

As another option, the impedance control approach proposed in [13] by Hogan is an effective way to simultaneously regulate the position and force without controller switching. In the impedance control approach, a compliant and delicate interaction control is achieved by constructing a virtual mass–spring–damper system that contains position error and interaction/contact force. In [14], Jung *et al.* designed a simple stable force tracking impedance control for a three-link robot manipulator that gets into contact with a rigid environment. In [15], Liaw and Shirinzadeh proposed a robust impedance control for a piezoactuated mechanism to deal with hysteresis, unknown force conversion function, and parametric uncertainties. In addition, Xu designed two discrete-time sliding-mode impedance controllers for microassembly in [16]. Note that if the environment model is known exactly, the compliant contact can be realized without exact force measurement. Nevertheless, in most of such developments, the contact environment is assumed as a simple mass–spring–damper or elastic system, which cannot adequately describe the actual environment accurately, especially for situations involving soft interaction.

In the field of robotic surgery, the position as well as the force exerted on the tissues is usually required to be regulated accurately. Thus, the formulation of the requirement for soft interaction between the device and human tissues (which are generally presented to be viscoelastic, nonlinear, and inhomogeneous) should be considered in order to attain proper and acceptable performance [17], [18]. Although some linear contact models (including the Maxwell model, the Kelvin–Voigt model, and the Kelvin–Boltzmann model) have been identified to describe this soft interaction and also used in the design of associated force controllers, such as disturbance observer [3], [17], and adaptive control [19], it is found that the Hunt–Crossley (HC) nonlinear model is rather more accurate for soft materials/environments such as breast tissue as well as tympanic membrane according to the comparative experiments in [20], [21]. In [18], a force controller based on HC model was proposed for minimally invasive robotic surgery, but unfortunately at that stage of development, this was only with step response tracking, and the position is not constrained. Therefore, the overall problem of dynamic contact on soft tissues continues to pose a new challenge on high-performance interaction control with both force and position

regulation. Moreover, there have not been too many efforts that have suitably and successfully further explored the effects of the HC model parameters on approaches with impedance control.

In the case of an ear surgical device, an ultrasonic motor driven by a piezoelectric actuator has been developed to complete the overall surgical process for the treatment of Otitis Media with Effusion (OME) [5], a prevailing disease that can result in hearing loss and body imbalance [22]. With such a system, the produced friction [23] typically deteriorates the performance of the device significantly. In [24]–[27], different control schemes and methods such as adaptive control, neural network control, and disturbance observer have been proposed and developed to compensate the aforementioned adverse impacts and to improve the position tracking accuracy. In [28]–[30], the robust integral of the sign of the error-based (RISE-based) adaptive controllers were developed for the hydraulic motion system to attain precise position tracking, but these methods cannot guarantee the finite-time convergence. However, it is worth noting that the position tracking is only one part of the ear surgical processes, and the force information should be incorporated into the designed controller so as to more appropriately complete the required complex task. This is particularly important for the required soft interaction with human tissues.

Motivated by the aforementioned essential issues, the overall control objective is to simultaneously regulate the force and position during the operating process for a soft interaction; and retain high robustness to the possibly adverse impacts arising from imperfections such as friction, hysteresis, and model uncertainties. Thus, in this article, a novel adaptive integral terminal sliding-mode-based impedance control (AITSMIC) is proposed to more suitably complete the operating processes of the piezoactuated ear surgical device in contact with soft tissues, which include contact, myringotomy, grommet insertion, and grommet release. The main contributions in theory of this article are listed as follows:

1) The rigorous development of an AITSMIC approach is proposed to comprehensively address the force and position tracking based on the more complete and more accurate HC nonlinear model, with rigorous analysis on attainment of steady-state performance. Along this line, this attained steady-state performance of the desired impedance model with soft tissues described by this nonlinear HC model is derived and analyzed to evaluate the steady-state position and force errors, and to facilitate parameter selection under soft interaction.

2) An integral terminal sliding manifold based on the auxiliary variable containing impedance error is developed to improve tracking performance and obtain finite-time convergence. An adaptive law is incorporated and augmented into the methodology to update the upper bound of the total disturbance to guarantee the robustness to undesired impacts with stability proof.

Also, the contributions in applications are verified via experiments.

1) The effectiveness of the impedance parameters is explored through position/force tracking experiments with soft interaction, and comparative results with other three
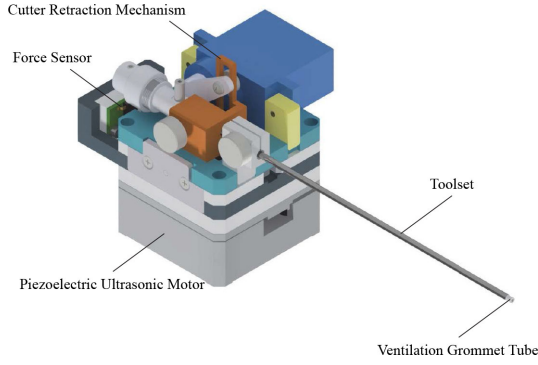
Fig. 1.   All-in-one piezoactuated ear surgical device.

controllers are demonstrated to evaluate the effectiveness of AITSMIC on dynamic force tracking.

2) The proposed method is employed in the surgical device to carry out a test surgical operation on a soft mock membrane to show the feasibility of appropriate and successful practical application.

In summary, the position and interaction force are controlled with only one uniform controller and without any switching between different control laws (which is straightforward for implementation); and the AITSMIC approach is also designed to be robust to nonlinearities (such as friction and hysteresis), unknown disturbances, and model parameter uncertainties.

The rest of this article is organized as follows. In Section II, the model of the piezoactuated ear surgical device is established. Section III presents the impedance model and steady-state error analysis with soft interaction. The detailed design of the proposed controller is then given in Section IV. Experimental setup and position/force tracking results on a piezoactuated ear surgical device are detailed and discussed in Section V, and finally, Section VI concludes this article.

II. PIEZOACTUATED EAR SURGICAL DEVICE

An all-in-one piezoactuated ear surgical device designed for automatically conducting the myringotomy with grommet insertion surgery to treat OME is shown in Fig. 1. It mainly includes a force-sensing system, a toolset (includes a cutter to process the myringotomy and a tube holder to insert the grommet), and a motion system (includes an ultrasonic motor to drive the overall toolset and a cutter retraction mechanism to move the cutter inside the tube holder). During the surgical operation, the piezoactuated ear surgical device driven by the ultrasonic motor moves the toolset and the attached tube to interact with the soft environment (i.e., tympanic membrane).

In general, a second-order system with the consideration of the friction, hysteresis as well as disturbances can be used to model this device [5], [31]. The second-order differential equation describing the ear surgical device model [32] is described by

$$m\ddot{x} + b\dot{x} + kx + f_c + f_h + f_{ed} = Tu - f_e \qquad (1)$$

where m is the effective mass, b is the effective damping coefficient, and k is the effective stiffness. x is the position measured by the linear encoder. $\dot{x}$ is the velocity and $\ddot{x}$ is the
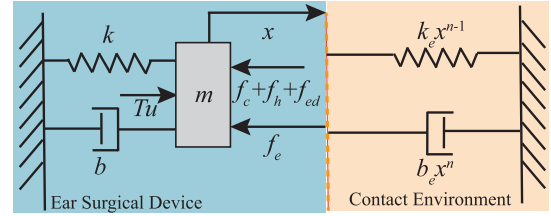

Fig. 2.   Diagram for the model of piezoactuated ear surgical device during contact.

acceleration. f_e is the interaction force between the environment and the device, which is measured by the force sensor. Moreover, u represents the input to the piezoelectric actuator and T is the system electromechanical ratio. f_c represents the friction, f_h represents the hysteresis, and f_{ed} represents the unknown disturbances, such as external disturbance and heat disturbance. The diagram for the model of piezoactuated ear surgical device in contact with the environment is demonstrated in Fig. 2, where k_e, b_e, and n are the soft tissue parameters.

Assumption 1 (see [32], [33]): f_c, f_h, and f_{ed} are bounded, which satisfy

$$|f_c| \le \Theta_c, |f_h| \le \Theta_h, |f_{ed}| \le \Theta_{ed} \qquad (2)$$

where $\Theta_c > 0$, $\Theta_h > 0$, $\Theta_{ed} > 0$ are constants.

Additionally, it is difficult to obtain the actual parameters of the system. Therefore, the nominal or identified plant is used for the controller design, and hence, the model uncertainties should be considered. The relationship between the actual parameters and the nominal parameters are shown as follows:

$$m = m_n + \Delta m, b = b_n + \Delta b, k = k_n + \Delta k \qquad (3)$$

where Δm, Δb, Δk represent the model uncertainties of the device and they are bounded by the upper bounds of Θ_m, Θ_b, Θ_k, respectively. Substituting (3) into (1), we can obtain

$$m_n\ddot{x} + b_n\dot{x} + k_nx + \Delta m\ddot{x} + \Delta b\dot{x}$$
$$+ \Delta kx + f_c + f_h + f_{ed} = Tu - f_e. \qquad (4)$$

Moreover, for practical applications, the measured x is usually filtered by a low-pass filter to reduce noises. Furthermore, the tracking trajectories in ear surgery are smooth or slow enough to avoid oscillation. Thus, the velocity and acceleration states are also bounded.

Assumption 2 (see [33], [34]): The model uncertainties $\Xi = \Delta m\ddot{x} + \Delta b\dot{x} + \Delta kx$ are bounded by

$$|\Xi| \le \Theta_m|\ddot{x}| + \Theta_b|\dot{x}| + \Theta_k|x| = \Theta_\Xi \qquad (5)$$

where Θ_Ξ is a constant that is positive.

Therefore, $f_t = \Delta m\ddot{x} + \Delta b\dot{x} + \Delta kx + f_c + f_h + f_{ed}$ gives the total disturbance, which is bounded by

$$|f_t| \le \Theta_{f_t} = \Theta_\Xi + \Theta_c + \Theta_h + \Theta_{ed}. \qquad (6)$$

It should be noted that the positive constant bound Θ_{f_t} is unknown. According to the aforementioned assumptions, the model of the piezoactuated ear surgical device is simplified as

$$m_n\ddot{x} + b_n\dot{x} + k_nx + f_t = Tu - f_e. \qquad (7)$$

With the given model (7), the analysis of the soft interaction and design of the controller can be established succinctly.

III. IMPEDANCE MODEL AND STEADY-STATE ERROR ANALYSIS WITH SOFT INTERACTION

To simultaneously regulate the position and force, the initial impedance model considering the position error and interaction force is formulated [13]. However, for the medical applications, it is also necessary to achieve the desired force response during the force tracking. Therefore, the target impedance model used in this article includes both position error and force error [14], which is given by

$$m_i \ddot{e}_p + b_i \dot{e}_p + k_i e_p = -k_f e_f \quad (8)$$

where m_i is desired inertia impedance parameter, b_i is desired damping impedance parameter, k_i is the desired stiffness impedance parameter. k_f is the parameter to adjust the weighting of force error. e_p and e_f are the position error and the interaction force error, respectively, which are given by

$$e_p = x - x_d, e_f = f_e - f_d \quad (9)$$

where x_d and f_d are the desired position and the desired force, respectively. Through the virtual relationship given in (8), the position and force can be simultaneously controlled with suitably selected impedance parameters.

The soft human tissues, such as tympanic membrane, present the viscoelastic, nonlinear, and inhomogeneous properties [20], [35]. According to our previous research and comparative experiments in [21], the HC model can be employed to obtain the behavior of soft interaction that is more in line with the physical intuition. The nonlinear HC model is described by

$$f_e = k_e(x - x_e)^n + b_e(x - x_e)^n \dot{x} \quad (10)$$

where x_e denoted the equilibrium position of the environment when the interaction force is absent. Compared with linear model, the equivalent damping and stiff coefficients, i.e., both $k_e(x - x_e)^{n-1}$ and $b_e(x - x_e)^n$ are dependent on the touch depth x. An illustration during the contact phase is given in Fig. 2 with $x_e = 0$ for conciseness.

Take the HC model (10) into the target impedance model (8), we can obtain

$$m_i \ddot{e}_p + b_i \dot{e}_p + k_i e_p = -k_f[k_e(x - x_e)^n + b_e(x - x_e)^n \dot{x} - f_d]. \quad (11)$$

It can be clearly found out that the equation is nonlinear, and therefore, it is hard to be solved. Therefore, the HC model is linearized [18] at first for the steady-steady performance analysis. Assuming that for the desired force f_d, the corresponding equilibrium position reaches at x_s. By applying Taylor series of x and $\dot{x}$ at x_s, we have

$$f_e(x, \dot{x}) \approx f_e(x_s, \dot{x}_s) + \left.\frac{\partial f_e}{\partial x}\right|_{x_s, \dot{x}_s} [(x - x_e) - (x_s - x_e)]$$

$$+ \left.\frac{\partial f_e}{\partial \dot{x}}\right|_{x_s, \dot{x}_s} [(\dot{x} - \dot{x}_e) - (\dot{x}_s - \dot{x}_e)]. \quad (12)$$

Furthermore, x_s can be also derived from (10) at the steady state, which is

$$f_d = k_e(x_s - x_e)^n + b_e(x_s - x_e)^n \dot{x}_s = k_e(x_s - x_e)^n$$

As a result

$$x_s = x_e + \sqrt[n]{\frac{f_d}{k_e}}. \quad (13)$$

By considering $\dot{x}_s = 0$ and (10), $\partial f_e/\partial x$ and $\partial f_e/\partial \dot{x}$ at $x_s, \dot{x}_s$ can be calculated as

$$\left.\frac{\partial f_e}{\partial x}\right|_{x_s, \dot{x}_s} = nk_e(x_s - x_e)^{n-1} + nb_e(x_s - x_n)^{n-1} \dot{x}_s$$

$$\approx nk_e(x_s - x_e)^{n-1} = nk_e \left(\frac{f_d}{k_e}\right)^{\frac{n-1}{n}} = \tilde{k}_e \quad (14)$$

and

$$\left.\frac{\partial f_e}{\partial \dot{x}}\right|_{x_s, \dot{x}_s} = b_e(x_s - x_e)^n = b_e \frac{f_d}{k_e} = \tilde{b}_e. \quad (15)$$

Combine (14) and (15), with (12), we can obtain

$$f_e(x, \dot{x}) \approx f_d + \tilde{k}_e(x - x_e) - \tilde{k}_e(x_s - x_e) + \tilde{b}_e \dot{x}. \quad (16)$$

Note that $\tilde{k}_e(x_s - x_e) = nf_d$ after appropriate simplifications of (13) and (14), and therefore, the linearized HC model is calculated as

$$f_e \approx f_d + \tilde{k}_e(x - x_e) - nf_d + \tilde{b}_e \dot{x}$$

$$\approx \tilde{k}_e(x - x_e) + \tilde{b}_e \dot{x} + (1 - n)f_d. \quad (17)$$

Thus, the dynamics for soft interaction with the target impedance (8) becomes

$$m_i \ddot{e}_p + b_i \dot{e}_p + k_i e_p \approx -k_f[\tilde{k}_e(x - x_e) + \tilde{b}_e \dot{x} + (1 - n)f_d - f_d]. \quad (18)$$

As $\ddot{x}_d, \dot{x}_d, \ddot{x}_e, \dot{x}_e, \ddot{x}$, and $\dot{x}$ all equal to zero for the steady-state response, the above-equation becomes

$$k_i e_p \approx -k_f \tilde{k}_e x + k_f \tilde{k}_e x_e + nk_f f_d,$$

$$\approx -k_f \tilde{k}_e e_p + k_f[nf_d + \tilde{k}_e(x_e - x_d)]. \quad (19)$$

Thus, the steady-state position error and the steady-state force error are obtained as shown in the following:

$$e_{pss} \approx \frac{k_f}{k_i + k_f \tilde{k}_e}[nf_d + \tilde{k}_e(x_e - x_d)]$$

$$e_{fss} \approx -\frac{k_i}{k_f} e_{pss} \approx -\frac{k_i}{k_i + k_f \tilde{k}_e}[nf_d + \tilde{k}_e(x_e - x_d)]. \quad (20)$$

From the aforementioned equations, it is found that for the soft interaction, e_{fss} is small if $k_i \ll k_f$, and the weighing of position performance is emphasized with $k_i \gg k_f$. Through selecting suitable impedance parameter, the steady-state performance can be adjusted for different tasks.

Remark 1: For some applications, the force-tracking performance is more important. According to (20), the system can

achieve the zero force steady-state error by

$$x_d = x_e + \frac{n f_d}{\tilde{k}_e}. \tag{21}$$

If the device can track the generated x_d, the desired interaction force is reached, which is similar to the methods shown in [32], i.e., position-based force-tracking impedance control. However, the accurate model of the environment, such as n, k_e, and b_e, should be known or identified online to achieve the desired performance, which increases the complexity of the control system significantly. Moreover, the dynamic trajectory tracking for the soft interaction cannot be realized due to the constant f_d in (21). Hence, the regulation of position and force is achieved by choosing impedance parameters in this article and only one uniform controller is designed to calculate the control input directly without the position inner-loop controller.

IV. CONTROLLER DESIGN

In this section, the design details of the novel adaptive robust impedance controller is presented.

A. Auxiliary Variable Definition

First, an auxiliary variable is defined based on the target impedance model (8) to facilitate the controller design, and the impedance error ϵ can be calculated as

$$\epsilon = m_i \ddot{e}_p + b_i \dot{e}_p + k_i e_p + k_f e_f. \tag{22}$$

To make the interaction process achieve the desired response, the control goal is to develop a controller so that $\lim_{t \to \infty} \epsilon \to 0$. By making

$$B_i = \frac{b_i}{m_i}, K_i = \frac{k_i}{m_i}, K_f = \frac{k_f}{m_i}$$

define an augmented impedance error as

$$\bar{\epsilon} = \ddot{e}_p + B_i \dot{e}_p + K_i e_p + K_f e_f. \tag{23}$$

Let us select two positive constants Λ and Γ that satisfy [8]

$$\Lambda + \Gamma = B_i, \Lambda\Gamma = K_i \tag{24}$$

and substitute them to (23), it yields

$$\bar{\epsilon} = \ddot{e}_p + (\Lambda + \Gamma)\dot{e}_p + \Lambda\Gamma e_p + K_f e_f. \tag{25}$$

Then, an auxiliary variable z is expressed as

$$z = \dot{e}_p + \Lambda e_p + e_l \tag{26}$$

where e_l satisfies

$$\dot{e}_l + \Gamma e_l = K_f e_f. \tag{27}$$

By taking (26) and (27) into (23), we can obtain

$$\bar{\epsilon} = \dot{z} + \Gamma z. \tag{28}$$

Hence, $z = 0$ will lead to $\epsilon = 0$ with the sequence that the control object becomes more compact by minimizing z.

Remark 2: For the selection of impedance parameters, i.e., m_i, b_i, k_i, the values should be assigned so that Λ and Γ exist according to (24). Therefore, these parameters are designed to satisfy

$$b_i^2 \geq 4 m_i k_i \tag{29}$$

and, thus, Λ and Γ are calculated by

$$\Lambda = \frac{m_i^{-1} b_i \pm \sqrt{m_i^{-2} b_i^2 - 4 m_i^{-1} k_i}}{2}$$
$$\tag{30}$$
$$\Gamma = \frac{m_i^{-1} b_i \mp \sqrt{m_i^{-2} b_i^2 - 4 m_i^{-1} k_i}}{2}.$$

B. Integral Terminal Sliding-Mode Controller

As the presence of complex and unknown disturbance such as friction in the piezoactuated ear surgical device, the controller should be designed to minimize the auxiliary variable z as well as to retain robust to these adverse impacts. Therefore, a novel integral terminal sliding manifold based on the auxiliary variable z is developed, which is defined as

$$\sigma = z + k_1 \int \left[z + k_2 \mathrm{sig}(z)^\rho\right] dt \tag{31}$$

where $\mathrm{sig}(\cdot)^\rho = |\cdot|^\rho \mathrm{sign}(\cdot)$, which is continuous and differentiable, $k_1 > 0$, $k_2 > 0$, and $0 < \rho < 1$. It is noteworthy that the integral action in the sliding function can help the control system to improve robustness to uncertainties and disturbances as well as steady-state performance [36], [37]. Furthermore, the finite-time convergence performance is guaranteed by the fractional-order term of sign error with the convergence time T_s, which can be calculated as

$$T_s \leq \frac{1}{k_1(1-\rho)} \ln \frac{2 k_1 V_{e,0}^{(1-\rho)/2} + 2^{(\rho+1)/2} k_2}{2^{(\rho+1)/2} k_2} \tag{32}$$

where $V_{e,0}$ is the initial value of $V_e = 1/2 z^2$.

By letting $\dot{\sigma} = 0$, $f_t = 0$ to derive the equivalent term u_{eq}, and adding the switching term u_{sw} to overcome external disturbances, the following theorem is developed.

Theorem 1: For the piezoactuated ear surgical device given by (7), the virtual variable z will converge to zero and achieve the target impedance if the following AITSMIC law with the integral terminal sliding function (9) is satisfied

$$u = u_{\mathrm{eq}} + u_{\mathrm{sw}} \tag{33}$$

and

$$u_{\mathrm{eq}} = \frac{m_n}{T}\left[\ddot{x}_d - \Lambda\dot{e}_p - \dot{e}_l - k_1 z - k_1 k_2 \mathrm{sig}(z)^\rho\right]$$
$$+ \frac{1}{T}(b_n \dot{x} + k_n x + f_e)$$

$$u_{\mathrm{sw}} = -\frac{1}{T}\hat{K}_s \mathrm{sign}(\sigma) \tag{34}$$

with the update law

$$\dot{\hat{K}}_s = \frac{\gamma}{m_n}|\sigma| \tag{35}$$

where $\gamma > 0$ is the adaptive gain.

Proof of Theorem 1. The control system stability is checked by the Lyapunov candidate function that is defined as

$$V = \frac{1}{2}\sigma^2 + \frac{1}{2\gamma}\tilde{K}_s^2 \tag{36}$$

where $\tilde{K}_s = \hat{K}_s - K_s$ is the estimated error of K_s to update the upper bound of the total disturbance f_t, and K_s satisfies the condition $|K_s| > \Theta_{f_t}$. It is clear that (36) is nonnegative and continuous, the time derivative of V is given as

$$\dot{V} = \sigma\dot{\sigma} + \gamma^{-1}(\hat{K}_s - K_s)\dot{\hat{K}}_s. \tag{37}$$

With (31), derivative σ with respect to time, then

$$\dot{\sigma} = \dot{z} + k_1 z + k_1 k_2 \text{sig}(z)^\rho$$

$$= \ddot{e}_p + \Lambda\dot{e}_p + \dot{e}_l + k_1 z + k_1 k_2 \text{sig}(z)^\rho \tag{38}$$

$$= \ddot{x} - \ddot{x}_d + \Lambda\dot{e}_p + \dot{e}_l + k_1 z + k_1 k_2 \text{sig}(z)^\rho.$$

According to the model (7), we can obtain that

$$\ddot{x} = \frac{1}{m_n}(Tu - b_n\dot{x} - k_n x - f_e - f_t). \tag{39}$$

Therefore, (38) becomes

$$\dot{\sigma} = \frac{1}{m_n}(Tu - b_n\dot{x} - k_n x - f_e - f_t) - \ddot{x}_d + \Lambda\dot{e}_p$$

$$+ \dot{e}_l + k_1 z + k_1 k_2 \text{sig}(z)^\rho \tag{40}$$

and $\dot{V}$ is derived as

$$\dot{V} = \sigma[\frac{1}{m_n}(Tu - b_n\dot{x} - k_n x - f_e - f_t) - \ddot{x}_d + \Lambda\dot{e}_p$$

$$+ \dot{e}_l + k_1 z + k_1 k_2 \text{sig}(z)^\rho] + \gamma^{-1}(\hat{K}_s - K_s)\dot{\hat{K}}_s. \tag{41}$$

Substitute the control law (33) and (34) into (41), we have

$$\dot{V} = -\frac{\sigma}{m_n}[\hat{K}_s\text{sign}(\sigma) + f_t] + \gamma^{-1}(\hat{K}_s - K_s)\dot{\hat{K}}_s. \tag{42}$$

By considering the adaptive law (35), it yields

$$\dot{V} = -\frac{\sigma}{m_n}[K_s\text{sign}(\sigma) + f_t] < 0 \tag{43}$$

with the condition $|K_s| > \Theta_{f_t}$.

Therefore, the sliding function σ will converge to zero so that the virtual variable z will also converge to zero in a finite time under (32) and achieve the target impedance. Also, the proposed AITSMIC retains robust to the unknown disturbance with the adaptive law to update the upper bound of the total disturbance real-time. □

It is observed from the aforementioned derivation that the auxiliary variable z is essential for the controller design, which makes the order of the impedance error reduce to a first-order equation by comparing (26) with (22), and can avoid the high-order derivative of x with the sliding manifold (31).

C. Overall Control Law

To avoid the estimated parameter $\hat{K}_s$ leading to unbounded values over time due to noise in (35), a projection operator is employed to alleviate this problem [38]. Considering that (32) is positive, with the upper bounds of K_s, i.e., $K_{s,\max}$, the modified adaptive law is given by

$$\dot{\hat{K}}_s = \text{Proj}_{\hat{K}_s}\left(\frac{\gamma}{m_n}|\sigma|\right) \tag{44}$$
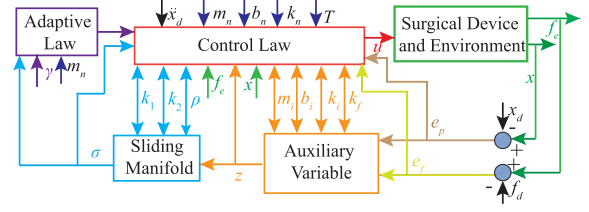

Fig. 3. Block diagram of the proposed AITSMIC scheme.

where

$$\text{Proj}_{\hat{K}_s}(\cdot) = \begin{cases} 0, & \text{if } \hat{K}_s = K_{s,\max} \text{ and } \cdot > 0 \\ \cdot, & \text{otherwise.} \end{cases} \tag{45}$$

Although we modify the adaptive low, the stability of Theorem 1 remains correct. This can be seen by the following.
1) If we have the condition *otherwise* in (45), the update law becomes $\dot{\hat{K}}_s = \frac{\gamma}{m_n}|\sigma|$. The stability is proved in Theorem 1 as shown in (43).
2) If $\hat{K}_s = K_{s,\max}$ and $\frac{\gamma}{m_n}|\sigma| > 0$, we have $\dot{\hat{K}}_s = 0$. Therefore, according to (42), it is deduced that

$$\dot{V} = -\frac{\sigma}{m_n}[K_{s,\max}\text{sign}(\sigma) + f_t]. \tag{46}$$

With the fact that $K_{s,\max} \geq K_s$, we have $\dot{V} < 0$. Therefore, the stability of the control low is still guaranteed through implementing the projection operator.

Additionally, e_l can be calculated by applying a filer $G_f(s)$ to e_f so as to avoid the derivative of signal and simplify the controller implementation. The transfer function $G_f(s)$ is given by the following equation based on (27):

$$G_f(s) = \frac{K_f}{s + \Gamma} \tag{47}$$

and $\dot{e}_l$ in (34) is obtained by

$$\dot{e}_l = K_f e_f - \Gamma e_l. \tag{48}$$

Finally, the following equation gives the overall control law:

$$u = \frac{m_n}{T}[\ddot{x}_d - \Lambda\dot{e}_p - K_f e_f + \Gamma e_l - k_1 z$$

$$- k_1 k_2 \text{sig}(z)^\rho] + \frac{1}{T}[b_m\dot{x} + k_n x + f_e - \hat{K}_s\text{sign}(\sigma)] \tag{49}$$

with the adaptive law (44).

Fig. 3 illustrates the overall block diagram of the proposed AITSMIC scheme including the parameters of the control scheme.

Remark 3: The proposed AITSMIC in this article generates the control force directly with respect to the impedance error, which is different from the controllers proposed in [14] and [32] where another position inner-loop controller is designed separately to track the virtual position trajectory. Moreover, the proposed method only involves one uniform controller to regulate and control both position and force, which is easier and more practical for implementation in comparison with the previous work presented in [3] and [11].
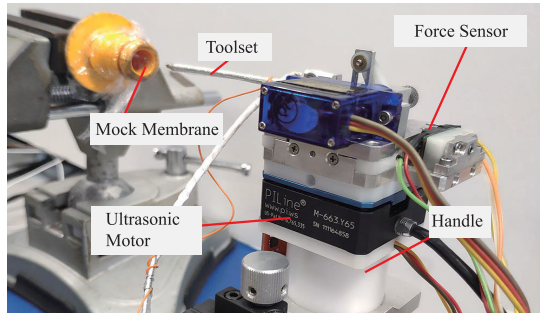
Fig. 4. Experimental platform of the piezoactuated ear surgical device.

Fig. 5. Tracking performance for S-curve of the proposed controller with different k_f. (a) Position-tracking results. (b) Force-tracking results.

Fig. 6. Trends and comparisons of position and force steady-state e_{rms} with different k_f.

Remark 4: The robustness of AITSMIC to unknown disturbance in the ear surgical device is also guaranteed by a sliding-mode technology without any complex modeling of the nonlinear effects.

V. EXPERIMENTAL RESULTS AND DISCUSSIONS

To evaluate the effectiveness and performance of the proposed method, an experimental platform is developed and three different experiments are carried out. The first experiment is to evaluate the effects of impedance parameters, the second experiment is to verify the tracking performance of the proposed controller and the last experiment is to validate the effectiveness on applying the proposed controller in the practical application (i.e., the ear surgical operation).

A. Experimental Setup

Fig. 4 shows the experimental platform. In this study, to simulate the human tympanic membrane (i.e., eardrum), a soft Polyethylene (PE) film with the similar mechanical properties to the human tympanic membrane is utilized as the mock membrane. The ultrasonic motor (PI-M663, Physik Instrumente) is used to drive the toolset to contact with the mock membrane, and a compact force sensor (FS1500NS, Honeywell) is integrated into the device to measure the interaction force between the toolset and the environment. The overall control system is implemented by the dSPACE DS1104 control card. The input voltage ranged from -10 to +10 V is generated to send to the motion controller (C-867, Physik Instrumente) through a digital-to-analog converter (DAC) and the position information is got from the linear encoder interface. The measured force is passed into the control system via an analog-to-digital converter (ADC). Through building the control blocks by MATLAB/Simulink, the real-time control system is developed. The sampling time is set at 1 ms. The nominal parameters are identified via the collected input–output data excited without any interaction, where a multifrequencies square wave is used as the input to avoid the effect of friction and hysteresis. Through the system identification toolbox in MATLAB, the system nominal parameters are obtained as $m_n = 1, b_n = 248.4, k_n = 202, T = 4940$.

Also, it should be noted that the toolset mounted on the motor will give rise to load uncertainty to the system. Furthermore, the friction and hysteresis will bring complex disturbances to the system.
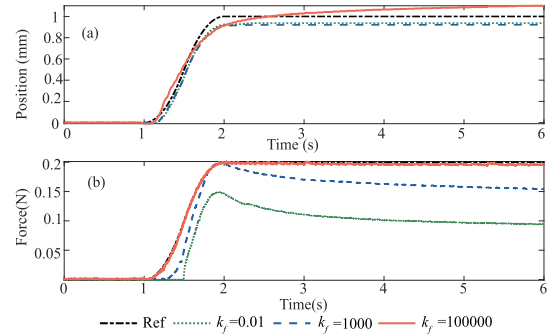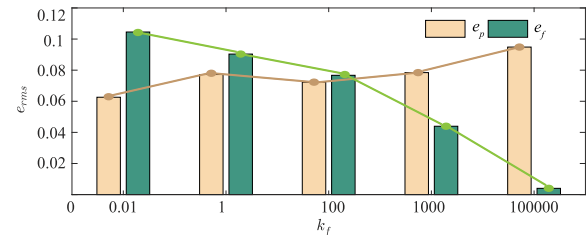
B. Effects of Impedance Parameter

To investigate the effects of impedance parameters, especially k_f, on the steady-state performance of position and interaction force, the toolset (see Fig. 4) is driven by the ultrasonic motor to contact with the soft mock membrane along a S-curve-like desired reference. The desired reference (Ref) is an S-curve with the rise time of 1 s, and subsequently retain at 1 mm and 0.2 N for position and force, respectively. For the parameters' selection in the control law, large values for those can lead to better steady-state performance and faster convergence but request an increased control input. Note that the too large integral coefficient k_2 may result in overshoot response. Therefore, in this article, $k_1 = 2000, k_2 = 0.02, \rho = 0.95, \gamma = 0.01$ are chosen. In addition, according to condition of (29), the impedance parameters m_i, b_i, k_i are chosen as 1100.53, and 2526.62, respectively to achieve the 8-Hz bandwidth of the impedance model. For a fair comparison, m_i, b_i, k_i are fixed while the parameter k_f varies from 0.01 to 100 000 so as to evaluate the effects of impedance parameter k_f on steady-state performance.

The position- and force-tracking results of the proposed controller for the S-curve are shown in Fig. 5, where k_f are set as 0.01, 1000, 100 000, respectively. For $k_f = 0.01$, the steady-state force is 0.098 N, whereas the steady-state position is 0.95 mm. The performance of force is deteriorated significantly for a smaller k_f. When k_f increases to 10 000, the steady-state value of force is 0.196 N in comparison with the value of position at 1.1 mm. Furthermore, the root-mean-square errors (e_{rms}) of the position and force at steady state are plotted in Fig. 6 for different k_f with different values. It is clear that the e_{rms} of force decreases significantly from 0.1045 to 0.0040 N with the increase of k_f. In contrast, e_{rms} of position increases from 0.0626 to 0.0949 mm.

TABLE I
PARAMETERS OF CONTROLLERS

Controller	Notation	Value
Impedance Model	m_i, b_i, k_i, k_f	1, 100.53, 2526.62, 100000
PIDIC	K_p, K_i, K_d	40.5, 160, 0.1
RSMIC	α, k_s, d, Δ	0.1, 0.01 , 0.001, 0.25
BCITSMC	$k_1, k_2, \rho, \lambda_1, \lambda_2$	0.01, 12, 1.02, 1, 1
	ξ_1, ξ_2, γ	0.1, 0.1, 0.01
AITSMIC	k_1, k_2, ρ, γ	2000, 0.02 ,0.95, 0.01

The experimental results in this section are consistent with the analysis in (20) for the steady-state performance. It should be noted that the force performance is more sensitive to the variation of k_f, and the position error always exits with the nonzero k_f.

C. Comparative Force Tracking Results

This subsection is to test and compare the tracking performance for the dynamic force. Here, the periodic S-curves with the same amplitude of 0.1 N but different frequency (0.25 Hz, 0.5 Hz, and 1 Hz) are set as the references. The experiments are performed during the interaction between the soft mock membrane and the device to verify the effectiveness of AITSMIC on tracking varying force.

For comparison purpose, another three controllers are also developed as the benchmarks. 1) The first one is the PID-based impedance control (PIDIC), where the PID position controller is designed and used to track the signal outputted by the virtual reference based on (8). The overall control scheme of PIDIC is similar to the methods presented in [14] and [39]. To improve the position-tracking performance, the linear–quadratic regulator (LQR) technique is employed to calculate the optimal control gains [31]. 2) Besides that, the robust sliding-mode impedance control (RSMIC) proposed in [15] is also used in this article, where the control force is calculated by the control law directly and no extra position controller is included. 3) Furthermore, an advanced integral backstepping impedance control with integral terminal sliding mode (BCITSMC) [40] is added to be compared in this section. The parameters of different controllers are all given in Table I. Here, it is noteworthy that the parameter k_f is chosen as 100 000 in order to compare the force-tracking performance.

Figs. 7–9 demonstrate the comparative tracking results of different controllers while the references at different frequencies are applied, respectively. Also, all the statistical force tracking results of different S-curves are listed in Table II. For 0.25 Hz (the lowest desired force tracking speed), both PIDIC and RSMIC obtain the similar e_{rms} of 0.0060 N and 0.0059 N, respectively. However, e_{max} of PIDIC is 0.0177 N, whereas the value of RSMIC is 0.0197 N. The performance of PIDIC is better than that of RSMIC. Significantly, e_{max} of PIDIC occurs in the rising phase of S-curve. This is because of the limited position bandwidth of the PID controller. In contrast, e_{max} of RSMIC occurs in the rising or falling phase, which is because there is significant impact from the friction. Actually, a suddenly changing disturbance to the system is induced by the variation of
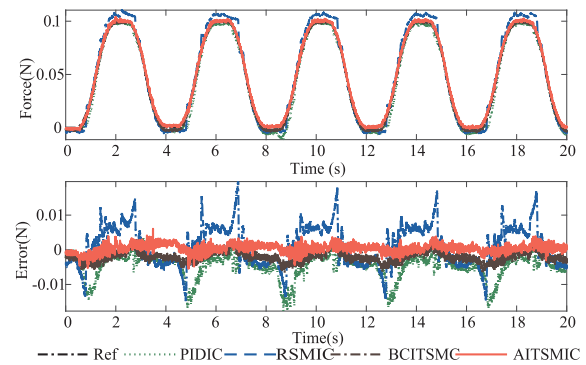

Fig. 7. Force-tracking performance of 0.25-Hz S-curve for different controllers. (a) Tracking results. (b) Tracking errors.
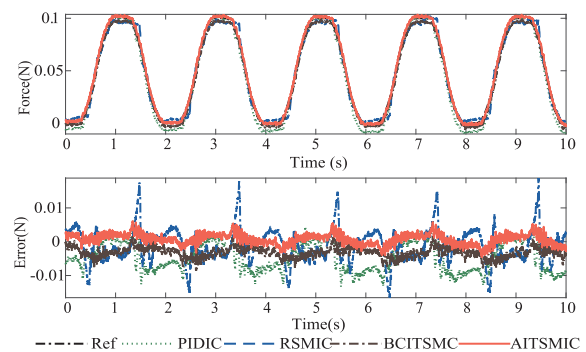

Fig. 8. Force-tracking performance of 0.5-Hz S-curve for different controllers. (a) Tracking results. (b) Tracking errors.
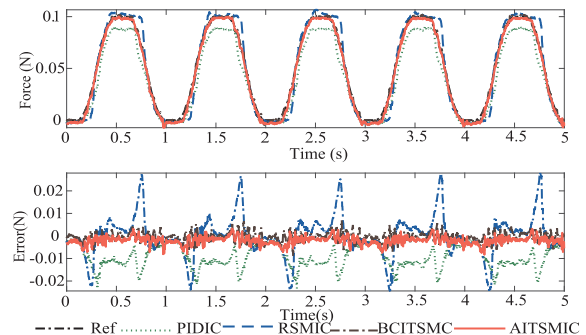

Fig. 9. Force-tracking performance of 1-Hz S-curve for different controllers. (a) Tracking results. (b) Tracking errors.

TABLE II
STATISTICAL FORCE-TRACKING RESULTS OF DIFFERENT S-CURVES

Errors (N)		0.25 Hz	0.5 Hz	1 Hz
PIDIC	e_{rms}	0.0060	0.0063	0.0106
	e_{max}	0.0177	0.0133	0.0234
RSMIC	e_{rms}	0.0059	0.0050	0.0088
	e_{max}	0.0197	0.0188	0.0279
BCITSMC	e_{rms}	0.0025	0.0036	0.0030
	e_{max}	0.0066	0.0086	0.0090
AITSMIC	e_{rms}	0.0025	0.0028	0.0027
	e_{max}	0.0061	0.0086	0.0083
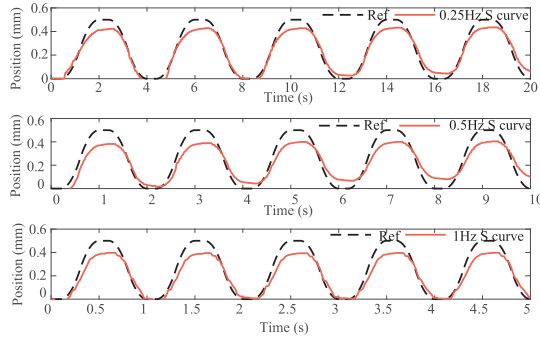
Fig. 10.   Measured position exerted on the mock membrane of the AITSMIC with different references.
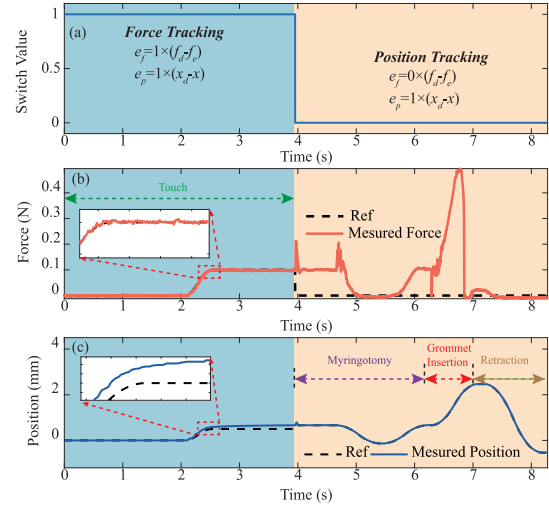

Fig. 11.   Experimental results and operating sequences of the surgical operation by applying the proposed AITSMIC. (a) Switching value between position and force. (b) Force-tracking result. (c) Position-tracking result.

dynamic motion direction, but the RSMIC cannot remove such a disturbance effectively because of the lack of integral action and adaptive term leading to low robustness to external disturbances. For the proposed method, e_{rms} and e_{max} are 0.0025 N and 0.0061 N, which improve 58.3% and 65.6% in comparison with PIDIC. Also note that the performance of BCITSMC is closed to that of AITSMIC at 0.25 Hz. The proposed method can compensate the adverse impact and track the reference precisely.

For results shown in Fig. 8, e_{max} of PIDIC at the 0.5-Hz S-curve is smaller than that of RSMIC, but e_{rms} is larger, which draws the same conclusion of the tracking results at 0.25 Hz. e_{rms} and e_{max} of BCITSMC reach 0.0036 N and 0.0086 N, respectively. The performance of AITSMIC remains the best with e_{rms} and e_{max} at 0.0028 N and 0.0086 N, respectively.

For the results shown in Fig. 9, the PIDIC performs the worst at 1 Hz, which steady-state force is 0.088 N. This is still due to its lower bandwidth. The results show that PIDIC cannot achieve the high-speed force trajectory tracking. For RSMIC, e_{rms} is 0.0088 N and e_{max} is 0.0279 N, whereas the problem of friction caused error still exists. Although the force-tracking performance of BCITSMC is improved significantly in comparison to PIDIC and RSMIC. The proposed method achieves e_{rms} of 0.0027 N and e_{max} of 0.0083 N, with the best performance among the four controllers, but with less parameters compared with BCITSMC.

When the references vary from 0.25 Hz to 1 Hz, all e_{rms} and e_{max} are within 0.003 N and 0.009 N, which are 3% and 9% of the reference stroke with AITSMIC. According to the aforementioned results, it is verified that the dynamic force can be tracked precisely under soft interaction by the proposed method with different frequencies.

The measured positions exerted on the soft mock membrane while applying the AITSMFC at different frequencies are also demonstrated in Fig. 10. Although the input references are standard S-curves, the measured positions with the precision force tracking are not exactly the same curves, which indicates that the soft mock membrane is nonlinear, viscoelastic, and inhomogeneous in characteristics as demonstrated in [21], and is different from the contact environment presented in [15] and [16]. Furthermore, the displacement depths vary with different contact speeds, approximate 0.42 mm, 0.40 mm, and 0.38 mm,

respectively. In spite of that, accurate force tracking with a relatively large impedance parameter can be achieved by the proposed methods.

D. Test Surgical Operation

This subsection validates the feasibility of the proposed controller in practical application. The piezoactuated ear surgical device is used in this validation. The surgical operation is called myringotomy with grommet insertion, where a grommet is inserted on a tympanic membrane and thus the fluid and pressure in the middle ear can be relieved. Significantly, the toolset mounted on the ultrasonic motor includes a cutter with a cutter retraction mechanism for incision making on the membrane and a hollow holder to push the grommet into the incision. The overall procedures include contact, myringotomy, grommet insertion and grommet release, during which the contact force and position should be controlled accurately enough to complete the surgery.

In the working process, first, the grommet is placed on the end of the toolset, and then, it is moved toward the membrane until the grommet touches the membrane at 0.1 N. During this phase, the precision tracking of force is important. A precise contact force can guarantee the success of grommet insertion. In other words, a small contact force will result in underinsertion while a large force will lead to overinsertion. Moreover, the position should also be constrained to ensure interaction stability, and the switching value is given as 1 for the controller to track the desired interaction force in Fig. 11(a). After the contact is stable, the process named myringotomy is stared. In this phase, the cutter retraction mechanism pushes out the cutter from the holder, and then, the cutter makes an incision on the soft membrane. Next, the device processes to the procedure for grommet insertion, the cutter is retracted by the cutter retraction mechanism and the holder is driven by the device to push the grommet into the incision. Finally, the overall process ends by the withdrawn
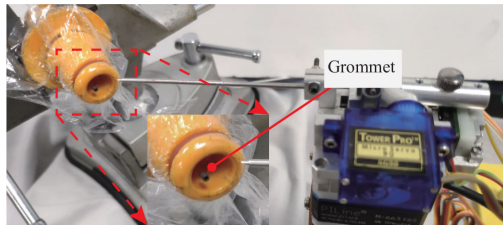
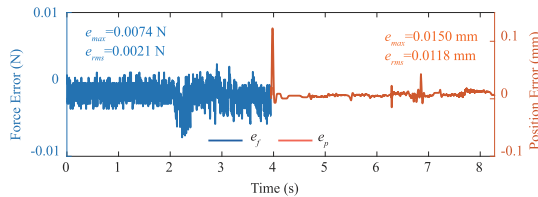Fig. 12. Successful surgical operation of inserting a grommet on mock membrane with the proposed method.

Fig. 13. Force and position errors during the surgical operation.

of the device without any touch. It is worth noting that for the myringotomy, grommet insertion, and withdrawn, the force information is only employed to monitor the value of force and supervise the action sequence. Therefore, the force error is set to be zero while the position is still used in the desired impedance model (8) to guarantee the position tracking accuracy as plotted in Fig. 11.

Fig. 11(b) and (c) demonstrates the force- and position-tracking performance, respectively. During the touch phase, the S-curves with a rising time of 0.5 s are set as the references with amplitudes of 0.1 N and 1 mm. It is clear that the interaction force tracks the reference precisely, whereas the measured position cannot reach the target position, which is in coincidence with the results of (20). For the position-tracking phase, the proposed AITSMIC tracks the position trajectory precisely so that the surgical operation can be completed successfully. The surgical operation is completed successfully where the grommet is inserted on the membrane correctly (see Fig. 12), and the stability can also be guaranteed by Theorem 1 because the controller is not changed.

The successful surgical operation of grommet insertion on a mock membrane with the proposed method is shown in Fig. 12. It is evident that the grommet is inserted on the membrane without underinsertion or overinsertion. It should be mentioned that the device also subjects to the time-varying disturbances due to the contact force with the membrane in the process of myringotomy with grommet insertion surgery. Fig. 13 plots the force and position errors during the overall operation, where e_{rms} and e_{max} of force are 0.0021 N and 0.0074 N, and those of position are 0.0150 mm and 0.0118 mm, respectively. These results indicate in the conclusion that the achieved force and position precision with the proposed controller can successfully complete the surgical operation via regulating the force and position simultaneously.

VI. CONCLUSION

In this article, an adaptive robust impedance control, i.e., AITSMIC, is developed for a piezoactuated ear surgical device to achieve successful surgical operations with control requirements of both force and position while the device is subjected to soft interaction. Because the soft human tissues are nonlinear, viscoelastic, and inhomogeneous in characteristics, the nonlinear HC model is used to investigate the effects of the target impedance model on the steady-state position and force performance. Furthermore, an auxiliary variable defined on basis of impedance error is designed to facilitate the controller design. Then, the accurate tracking performance on the desired reference as well as the finite-time convergence is guaranteed by an integral-type terminal sliding manifold. An adaptive law is designed to estimate the upper bound of the total disturbance to deal with the system nonlinearities, disturbances, and model uncertainties, which are imperfections typically presented in piezoelectric actuators. The stability of the proposed control system is also carefully proven by the Lyapunov theory. Moreover, the effects of impedance parameters on the steady-state position error as well as the steady-state force error are evaluated by force/position tracking experiments with soft interaction. The dynamic force-tracking performance of AITSMIC is also verified by comparing with three benchmark controllers from different references, where AITSMIC achieves the best tracking performance and its e_{rms} and e_{max} are within 3% and 9% of the reference stroke. Finally, the proposed method is applied on the test surgical device and the test surgical operation on the mock membrane can be completed successfully, which shows the feasibility of the proposed method in practical application.

REFERENCES

[1] D. Kim, K. Koh, G. R. Cho, and L.-Q. Zhang, "A robust impedance controller design for series elastic actuators using the singular perturbation theory," *IEEE/ASME Trans. Mechatronics*, vol. 25, no. 1, pp. 164–174, Feb. 2020.

[2] H. B. Huang, D. Sun, J. K. Mills, and S. H. Cheng, "Robotic cell injection system with position and force control: Toward automatic batch bioma-nipulation," *IEEE Trans. Robot.*, vol. 25, no. 3, pp. 727–737, Jun. 2009.

[3] W. Liang, J. Ma, and K. K. Tan, "Contact force control on soft membrane for an ear surgical device," *IEEE Trans. Ind. Electron.*, vol. 65, no. 12, pp. 9593–9603, Dec. 2018.

[4] F. Ferraguti, C. T. Landi, L. Sabattini, M. Bonfé, C. Fantuzzi, and C. Secchi, "A variable admittance control strategy for stable physical human-robot interaction," *Int. J. Robot. Res.*, vol. 38, no. 6, pp. 747–765, 2019.

[5] K. K Tan, W. Liang, P. Le Pham, S. Huang, C. W. Gan, and H. Y. Lim, "Design of a surgical device for office-based myringotomy and grommet insertion for patients with otitis media with effusion," *J. Med. Devices*, vol. 8, no. 3, 2014, Art. no. 031001.

[6] Z. Zarrouk, A. Chemori, and P. Poignet, "Adaptive force feedback control for 3D compensation of physiological motion in beating heart surgery," in *Proc. IEEE/RSJ Int. Conf. Intell. Robots Syst.*, 2010, pp. 1856–1861.

[7] J. Lee, M. Jin, N. Kashiri, D. G. Caldwell, and N. G. Tsagarakis, "Inversion-free force tracking control of piezoelectric actuators using fast finite-time integral terminal sliding-mode," *Mechatronics*, vol. 57, pp. 39–50, 2019.

[8] Y. Li, S. S Ge, and C. Yang, "Learning impedance control for physical robot-environment interaction," *Int. J. Control*, vol. 85, no. 2, pp. 182–193, 2012.

[9] M. Madani and M. Moallem, "Hybrid position/force control of a flexible parallel manipulator," *J. Franklin Inst.*, vol. 348, no. 6, pp. 999–1012, 2011.

[10] G. Wang and Q. Xu, "Design and precision position/force control of a piezo-driven microinjection system," *IEEE/ASME Trans. Mechatronics*, vol. 22, no. 4, pp. 1744–1754, 2017.

[11] W. Liang and K. K. Tan, "Force feedback control assisted tympanostomy tube insertion," *IEEE Trans. Control Syst. Technol.*, vol. 25, no. 3, pp. 1007–1018, May 2017.

[12] T. Kim, S. Yoo, T. Seo, H. S. Kim, and J. Kim, "Design and force-tracking impedance control of 2-DOF wall-cleaning manipulator via disturbance observer," *IEEE/ASME Trans. Mechatronics*, vol. 25, no. 3, pp. 1487–1498, Jun.2020.

[13] N. Hogan, "Impedance control: An approach to manipulation," *J. Dyn. Syst., Meas., Control*, vol. 107, pp. 1–24, 1985.

[14] S. Jung, T. C. Hsia, and R. G. Bonitz, "Force tracking impedance control for robot manipulators with an unknown environment: Theory, simulation, and experiment," *Int. J. Robot. Res.*, vol. 20, no. 9, pp. 765–774, 2001.

[15] H. C. Liaw and B. Shirinzadeh, "Robust generalised impedance control of piezo-actuated flexure-based four-bar mechanisms for micro/nano manipulation," *Sensors Actuators A: Phys.*, vol. 148, no. 2, pp. 443–453, 2008.

[16] Q. Xu, "Precision position/force interaction control of a piezoelectric multimorph microgripper for microassembly," *IEEE Trans. Autom. Sci. Eng.*, vol. 10, no. 3, pp. 503–514, Jul. 2013.

[17] P. Moreira, N. Zemiti, C. Liu, and P. Poignet, "Viscoelastic model based force control for soft tissue interaction and its application in physiological motion compensation," *Comput. Methods Programs Biomed.*, vol. 116, no. 2, pp. 52–67, 2014.

[18] A. Pappalardo, A. Albakri, C. Liu, L. Bascetta, E. De Momi, and P. Poignet, "Hunt-Crossley model based force control for minimally invasive robotic surgery," *Biomed. Signal Process. Control*, vol. 29, pp. 31–43, 2016.

[19] C. Liu, P. Moreira, and P. Poignet, "Viscoelastic model based force tracking control for robotic-assisted surgery," in *Proc. 4th IEEE RAS EMBS Int. Conf. Biomed. Robot. Biomechatronics*, 2012, pp. 1199–1204.

[20] R. Schindeler and K. Hashtrudi-Zaad, "Online identification of environment Hunt-Crossley models using polynomial linearization," *IEEE Trans. Robot.*, vol. 34, no. 2, pp. 447–458, Apr. 2018.

[21] C. Ng, W. Liang, C. W. Gan, H. Y. Lim, and K. K. Tan, "Optimization of the penetrative path during grommet insertion in a robotic ear surgery," *Mechatronics*, vol. 60, pp. 1–14, 2019.

[22] H. Atkinson, S. Wallis, and A. P. Coatesworth, "Otitis media with effusion," *Postgraduate Med.*, vol. 127, no. 4, pp. 381–385, 2015.

[23] S. Huang, W. Liang, and K. K. Tan, "Intelligent friction compensation: A review," *IEEE/ASME Trans. Mechatronics*, vol. 24, no. 4, pp. 1763–1774, Aug. 2019.

[24] J. Y. Lau, W. Liang, H. C. Liaw, and K. K. Tan, "Sliding mode disturbance observer-based motion control for a piezoelectric actuator-based surgical device," *Asian J. Control*, vol. 20, no. 3, pp. 1194–1203, 2018.

[25] W. Liang, J. Ma, C. Ng, Q. Ren, S. Huang, and K. K. Tan, "Optimal and intelligent motion control scheme for an ultrasonic-motor-driven XY stage," *Mechatronics*, vol. 59, pp. 127–139, 2019.

[26] Z. Feng, J. Ling, M. Ming, and X. Xiao, "Integrated modified repetitive control with disturbance observer of piezoelectric nanopositioning stages for high-speed and precision motion," *J. Dyn. Syst., Meas., Control*, vol. 141, no. 8, 2019, Art. no. 0 81006.

[27] Z. Feng, J. Ling, M. Ming, W. Liang, K. K. Tan, and X. Xiao, "Signal-transformation-based repetitive control of spiral trajectory for piezoelectric nanopositioning stages," *IEEE/ASME Trans. Mechatronics*, vol. 25, no. 3, pp. 1634–1645, Jun. 2020.

[28] J. Yao, Z. Jiao, D. Ma, and L. Yan, "High-accuracy tracking control of hydraulic rotary actuators with modeling uncertainties," *IEEE/ASME Trans. Mechatronics*, vol. 19, no. 2, pp. 633–641, Apr. 2014.

[29] J. Yao, W. Deng, and Z. Jiao, "Rise-based adaptive control of hydraulic systems with asymptotic tracking," *IEEE Trans. Autom. Sci. Eng.*, vol. 14, no. 3, pp. 1524–1531, Jul. 2017.

[30] W. Deng and J. Yao, "Adaptive integral robust control and application to electromechanical servo systems," *ISA Trans.*, vol. 67, pp. 256–265, 2017.

[31] K. K. Tan *et al.*, "Precision control of piezoelectric ultrasonic motor for myringotomy with tube insertion," *J. Dyn. Syst., Meas., Control*, vol. 137, no. 6, 2015, Art. no. 064504.

[32] J. Y. Lau, W. Liang, and K. K. Tan, "Enhanced robust impedance control of a constrained piezoelectric actuator-based surgical device," *Sensors Actuators A, Phys.*, vol. 190, pp. 97–106, 2019.

[33] A. Al-Ghanimi, J. Zheng, and Z. Man, "A fast non-singular terminal sliding mode control based on perturbation estimation for piezoelectric actuators systems," *Int. J. Control*, vol. 90, no. 3, pp. 480–491, 2017.

[34] A. Safa, R. Y. Abdolmaleki, and H. C. Nejad, "Precise position tracking control with an improved transient performance for a linear piezoelectric ceramic motor," *IEEE Trans. Ind. Electron.*, vol. 66, no. 4, pp. 3008–3018, Apr. 2019.

[35] A. Haddadi and K. Hashtrudi-Zaad, "Real-time identification of Hunt-Crossley dynamic models of contact environments," *IEEE Trans. Robot.*, vol. 28, no. 3, pp. 555–566, Jun. 2012.

[36] Y. Lee, S. H. Kim, and C. C. Chung, "Integral sliding mode control with a disturbance observer for next-generation servo track writing," *Mechatronics*, vol. 40, pp. 106–114, 2016.

[37] Z. Feng, W. Liang, J. Ling, X. Xiao, K. K. Tan, and T. H. Lee, "Integral terminal sliding-mode-based adaptive integral backstepping control for precision motion of a piezoelectric ultrasonic motor," *Mech. Syst. Signal Process.*, vol. 144, 2020, Art. no. 106856.

[38] S. Bashash and N. Jalili, "Robust adaptive control of coupled parallel piezo-flexural nanopositioning stages," *IEEE/ASME Trans. Mechatronics*, vol. 14, no. 1, pp. 11–20, Feb. 2009.

[39] J. Duan, Y. Gan, M. Chen, and X. Dai, "Adaptive variable impedance control for dynamic contact force tracking in uncertain environment," *Robot. Auton. Syst.*, vol. 102, pp. 54–65, 2018.

[40] W. Liang, Z. Feng, Y. Wu, J. Gao, Q. Ren, and T. H. Lee, "Robust force tracking impedance control of an ultrasonic motor-actuated end-effector in a soft environment," in *Proc. IEEE/RSJ Int. Conf. Intell. Robots Syst.*, 2020, pp. 7716–7722.
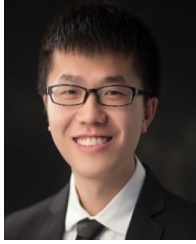
Zhao Feng received the B.S. degree from the School of Power and Mechanical Engineering, Wuhan University, Wuhan, China, in 2014, and the Ph.D. degree from Wuhan University in 2020, both in mechanical engineering .

His research interests include vibration control, iterative learning control, nanopositioning, and robotics.

Wenyu Liang (Member, IEEE) received the B.Eng. and M.Eng. degrees from the China Agricultural University, Beijing, China, in 2008 and 2010, respectively, both in mechanical engineering, and the Ph.D. degree in electrical and computer engineering from the National University of Singapore (NUS), Singapore, in 2014.

He is currently a Scientist with the Institute for Infocomm Research, A*STAR, Singapore, and also an Adjunct Assistant Professor with the Department of Electrical and Computer Engineering, NUS. His research interests mainly include robotics, intelligent systems, precision motion control, and force control.

Jie Ling (Member, IEEE) received the B.S. and Ph.D. degrees from the School of Power and Mechanical Engineering, Wuhan University, Wuhan, China, in 2012 and 2018, respectively, both in mechanical engineering.

He was a Visiting Ph.D. Student with the Department of Automatic Control and Micro-Mechatronic Systems, FEMTO-st Institute, France, in 2017. From 2019 to 2020, he was a Postdoc Researcher with the Department of Biomedical Engineering, National University of Singapore, Singapore. Since 2020, he has been an Associate Professor with the College of Mechanical and Electrical Engineering, Nanjing University of Aeronautics and Astronautics. His research interests include mechanical design and precision motion control of nanopositioning stages and micromanipulation robots.

Xiaohui Xiao (Member, IEEE) received the B.S. and M.S. degrees from Wuhan University, Wuhan, China, in 1991 and 1998, respectively, and the Ph.D. degree from the Huazhong University of Science and Technology, Wuhan, in 2005, all in mechanical engineering.

In 1998, she joined Wuhan University, Wuhan, China, where she is currently a Full Professor with the Mechanical Engineering Department, School of Power and Mechanical Engineering. She has authored/coauthored more than 30 papers in the areas of mobile robots, dynamics and control, sensors, and signal procession. Her current research interests include mobile robotics, high-precision positioning control, and signal processing.

Kok Kiong Tan received the B.Eng. and Ph.D. degrees from the Department of Electrical and Computer Engineering, National University of Singapore, Singapore, in 1992 and 1995, respectively, both in electrical and computer engineering.

Prior to joining the National University of Singapore, he was a Research Fellow with the Singapore Institute of Manufacturing Technology, Singapore, a national R&D institute spearheading the promotion of R&D in local manufacturing industries, where he was involved in managing industrial projects. He was a Professor with the National University of Singapore, and is currently with ZAI company. His research interests include precision motion control and instrumentation, advanced process control and autotuning, and general industrial automation.

Tong Heng Lee (Member, IEEE) received the B.A. with first class Hons. degree in engineering tripos from Cambridge University, Cambridge, U.K., in 1980, and the Ph.D. degree in electrical engineering from Yale University, New Haven, CT, USA, in 1987.

He is currently a Professor with the Department of Electrical and Computer Engineering, National University of Singapore, Singapore. His research interests include the areas of adaptive systems, knowledge-based control, intelligent mechatronics, and computational intelligence. He currently holds Associate Editor appointments in the IEEE TRANSACTIONS IN SYSTEMS, MAN AND CYBERNETICS; the *Control Engineering Practice* (an IFAC journal); and is a Consulting Editor for the *International Journal of Systems Science* (Taylor and Francis, London). In addition, he is the past Deputy Editor-in-Chief of IFAC Mechatronics journal. He has also coauthored five research monographs (books), and holds four patents (two of which are in the technology area of adaptive systems, and the other two are in the area of intelligent mechatronics).

Dr. Lee was an Invited Panelist, an Invited Keynote Speaker for many international conferences. He was a recipient of the Cambridge University Charles Baker Prize in Engineering and several best conference paper prizes. He was also a multiple winner of the National University of Singapore FoE Engineering Educator Award, and is currently on the Engineering Educator Honor Roll.